Electronic Supporting Information for

In-silico design of porous polymer networks: high-throughput screening for methane storage materials

Richard L. Martin, Cory M. Simon, Berend Smit and Maciej Haranczyk

This document provides the following supporting information:

- Comparison of simulated and experimental adsorption data
- Additional data for the spherical shell model
- Further plots for understanding the performance arc comparing DC(35,1) and DC(65,5.8)
- Additional plots of structure-property relationships for both geometric and chemical descriptors

Comparison to experimental adsorption data

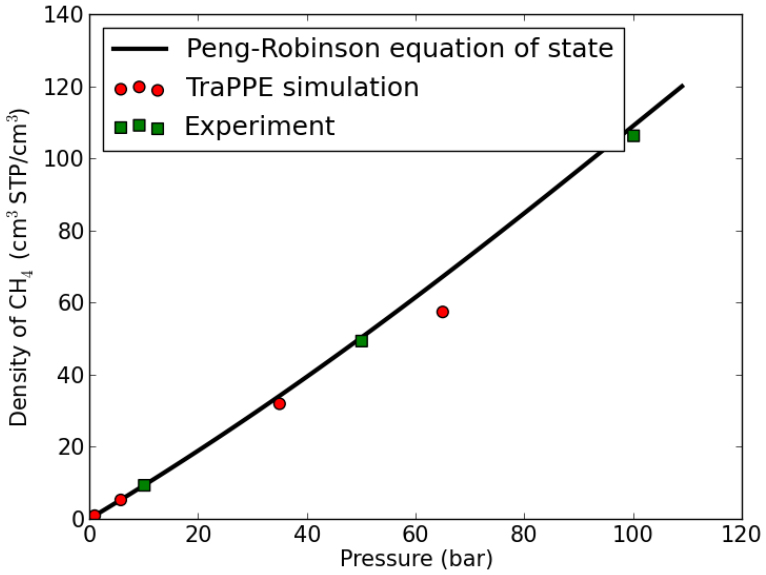

Figure S1. Validating the TraPPE model and Peng-Robinson equation of state at 298 K. Green squares are experimental measurements of methane density as a function of pressure[45]. The black curve is the calculation using the Peng-Robinson equation of state. Red circles are calculations from Grand-canonical Monte Carlo simulations in an empty box (i.e., no adsorbent framework) using the TraPPE potential for methane.

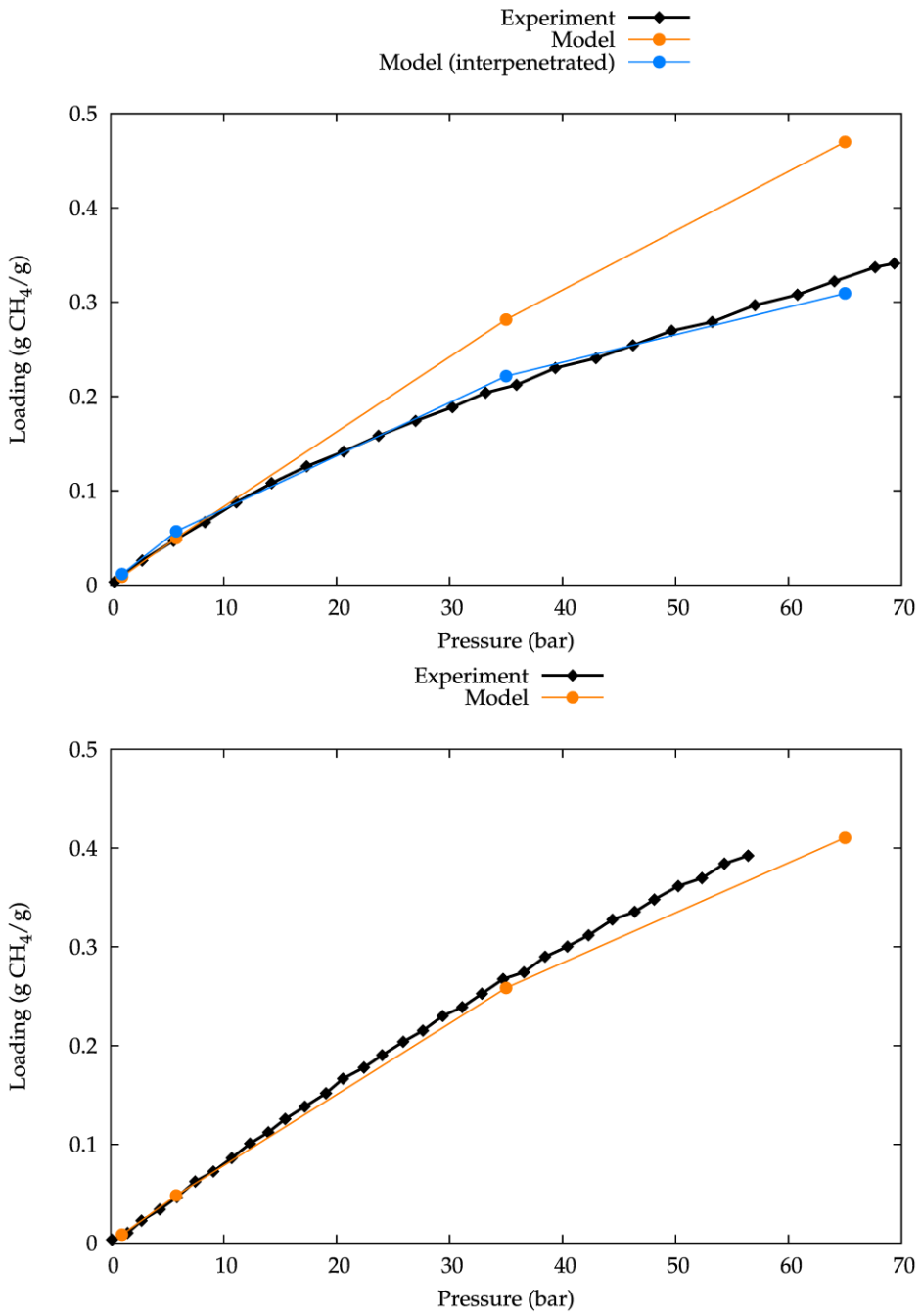

Figure S2. PPN-3 (interpenetrated model, above) and PPN-4 (below) simulated methane adsorption data are shown to exhibit strong agreement with experimental measurements.

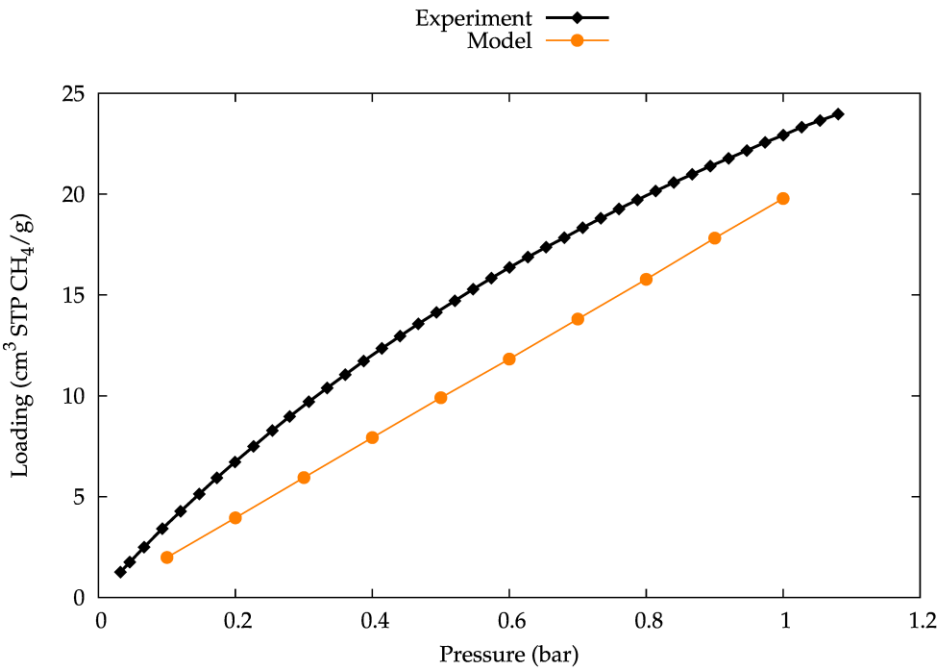

Figure S3. PPN-101 simulated methane adsorption data is shown to exhibit good qualitative agreement with experimental measurements.

Spherical shell model

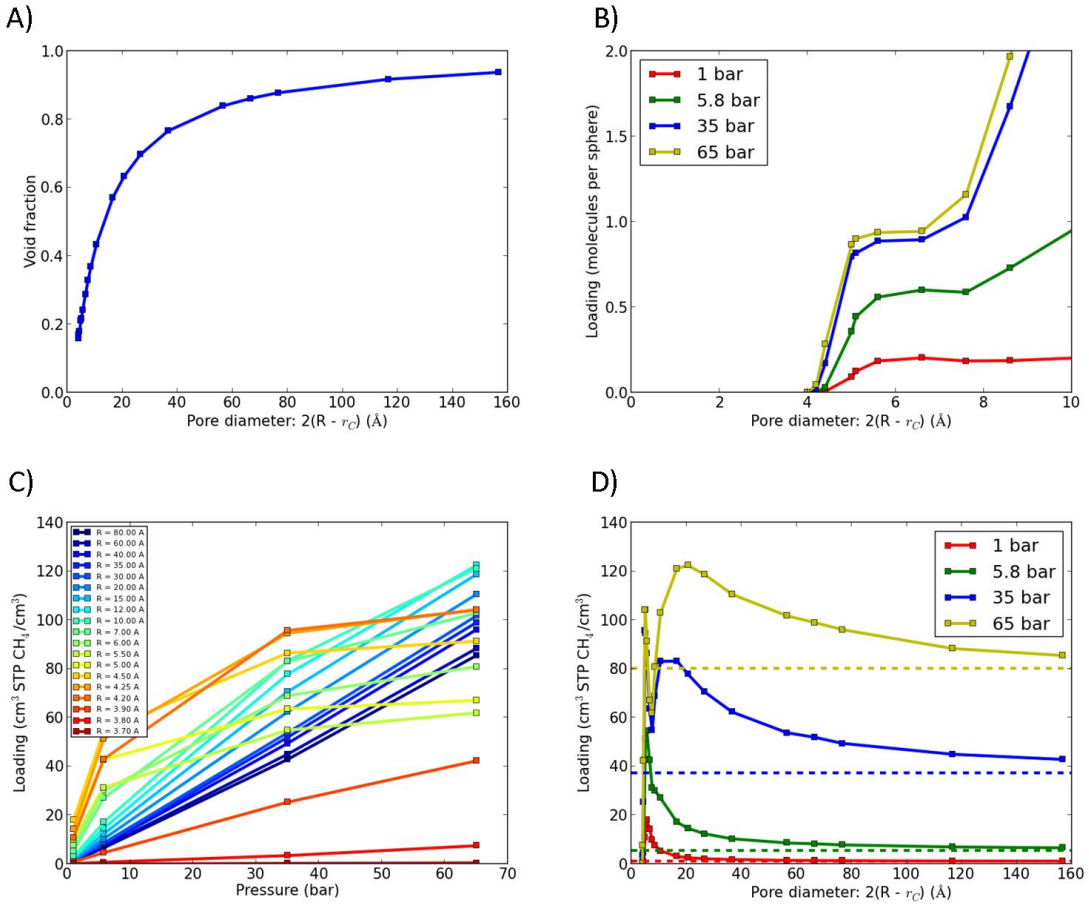

Figure S4. A) The free volume of our model material increases with increasing pore size, as the carbon atoms in the shell occupy a lesser fraction of the material volume. Here, the void fraction of our material is defined as the volume in a sphere of radius (R-r_c) divided by the unit cell volume, a sphere of radius R. The quantity r_c = 1.7 Å is the van der Waals radius of carbon. B) The methane loading (in units of molecules per unit cell of our model material) as a function of pore diameter. Colors distinguish different pressures. A plateau occurs in the approximate diameter range of 5-7 Å, where the pore becomes large enough for one methane to fit, but not large enough for dual occupancy. As a result, there is little change in loading when the pore size increases from single to double methane capacity. C) Computed methane adsorption isotherms for models of varying radii. D) Computed methane loading at four different pressures as a function of the model pore size. Horizontal dashed lines indicate the density of bulk methane gas at the respective pressures.

Understanding the performance arc

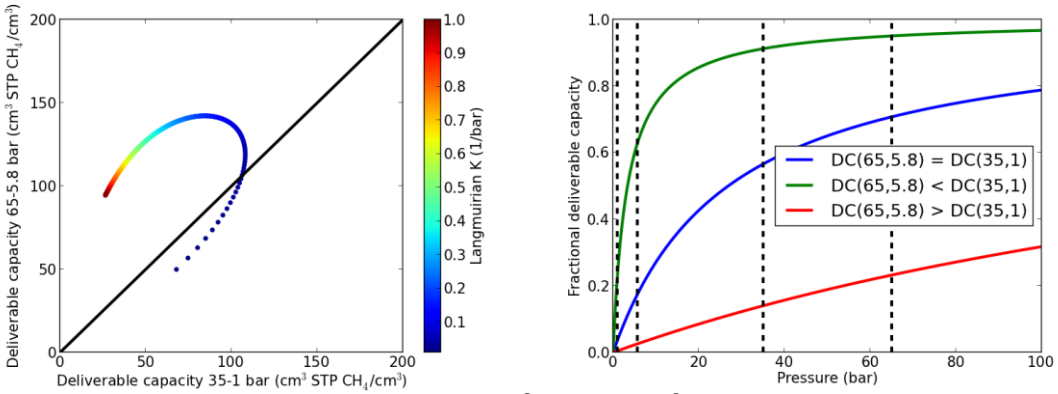

Figure S5. Left: at fixed saturation loading (200 cm^3_{STP} $(CH_4)/cm^3$), altering the Langmuirian constant *K* reproduces, qualitatively, the 'performance curve' identified in Figure 5 (warmer colors indicating saturation at a lower pressure). Right: the isotherm for the *K* which provides equal DC(35,1) and DC(65,5.8) is shown in blue; isotherms based on altering *K* from this point by a factor of 8, illustrating preference towards DC(35,1) (green) and DC(65,5.8) (red), are also shown. Vertical dashed lines show pressures of interest.

Further structure-property relationship plots

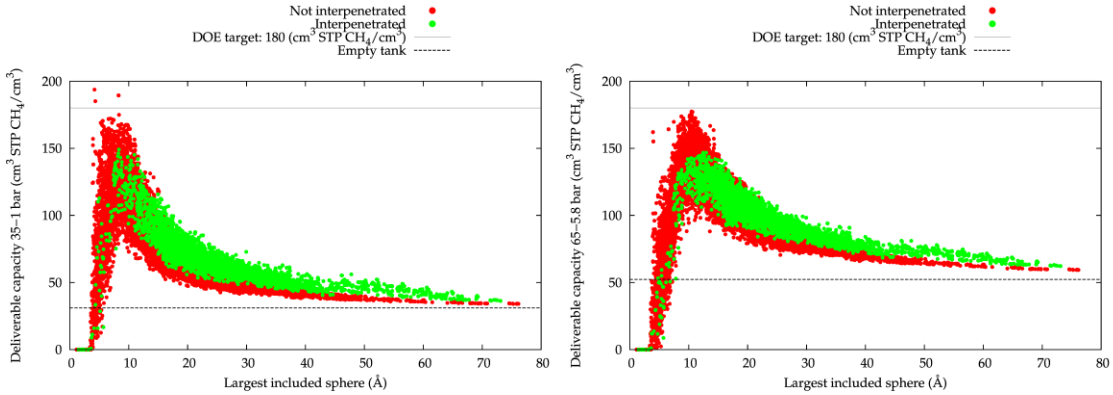

Figure S6. DC(35,1), left, and DC(65,5.8), right, as a function of largest included sphere diameter, color-coded by the presence of interpenetration.

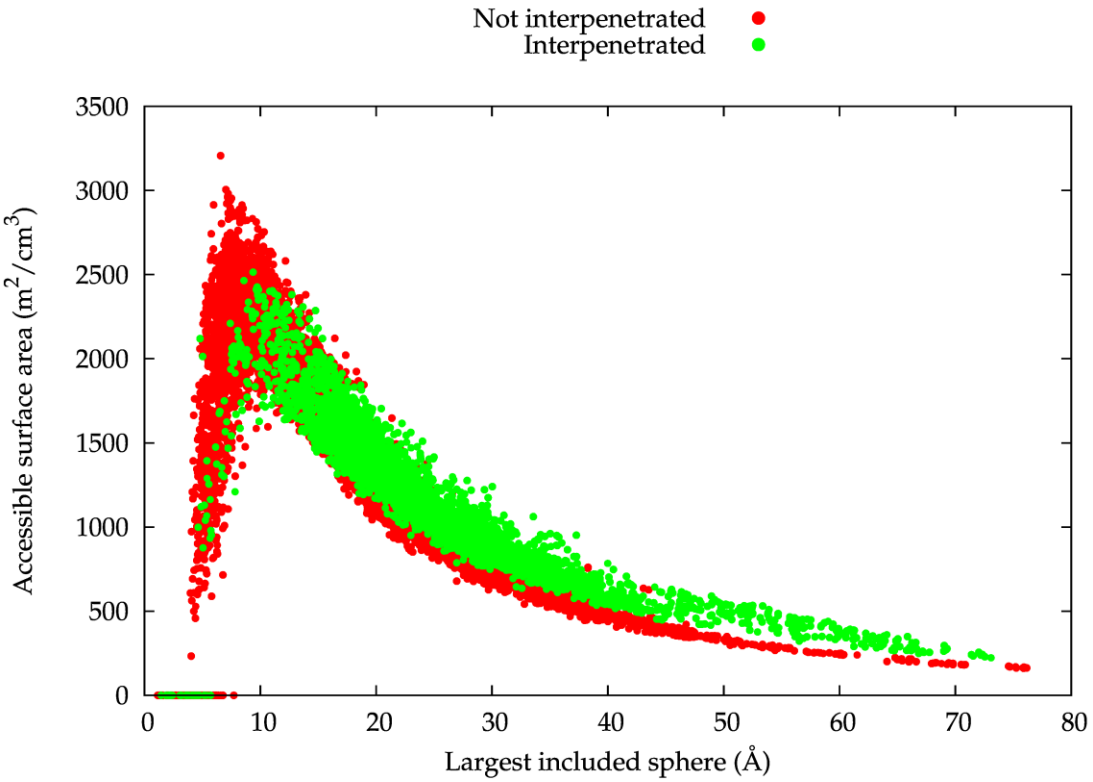

Figure S7. Surface area as a function of largest included sphere diameter, for interpenetrated versus non-interpenetrated materials.

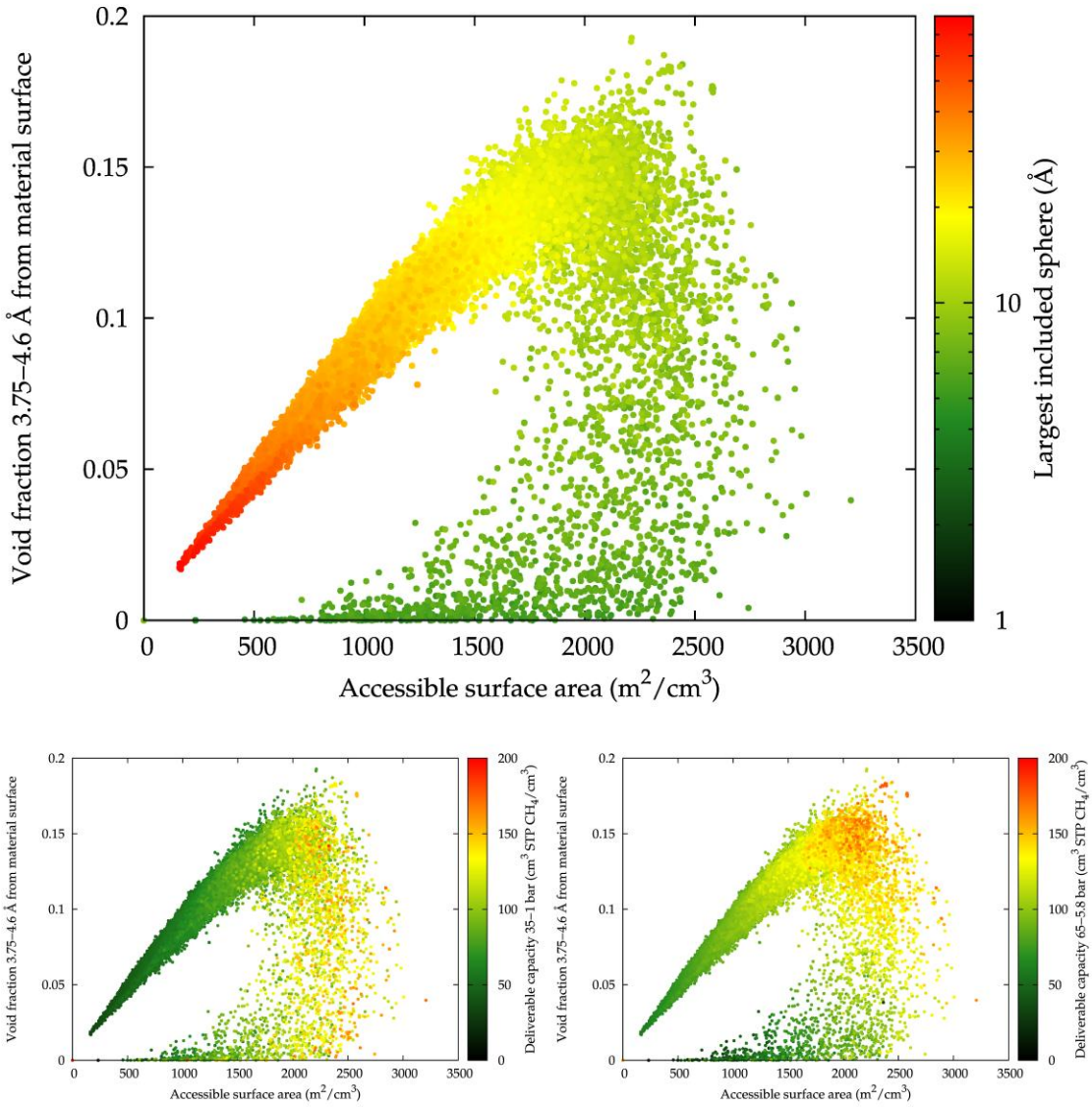

Figure S8. Above: the relationship between volumetric surface area and van der Waals void fraction (WVF), color-coded by largest pore diameter. Below: alternative color-codings, illustrating that while the WVF has little correlation with DC(35,1), the best DC(65,5.8) structures exhibit a high WVF.

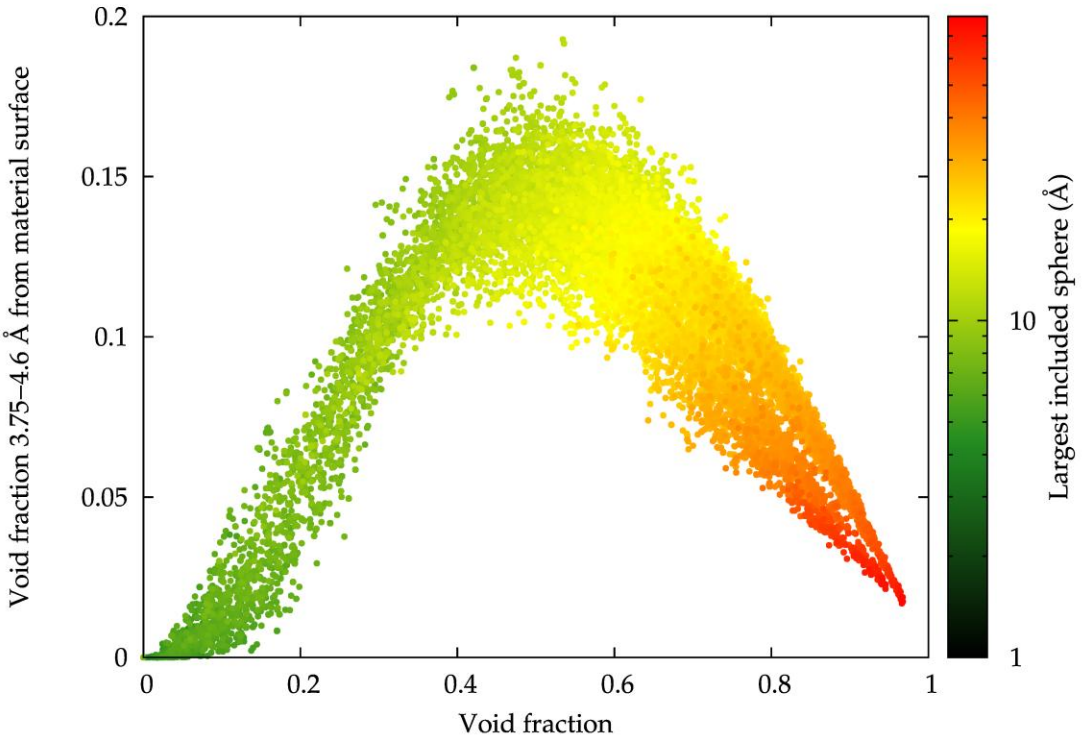

Figure S9. The relationship between void fraction and van der Waals void fraction.

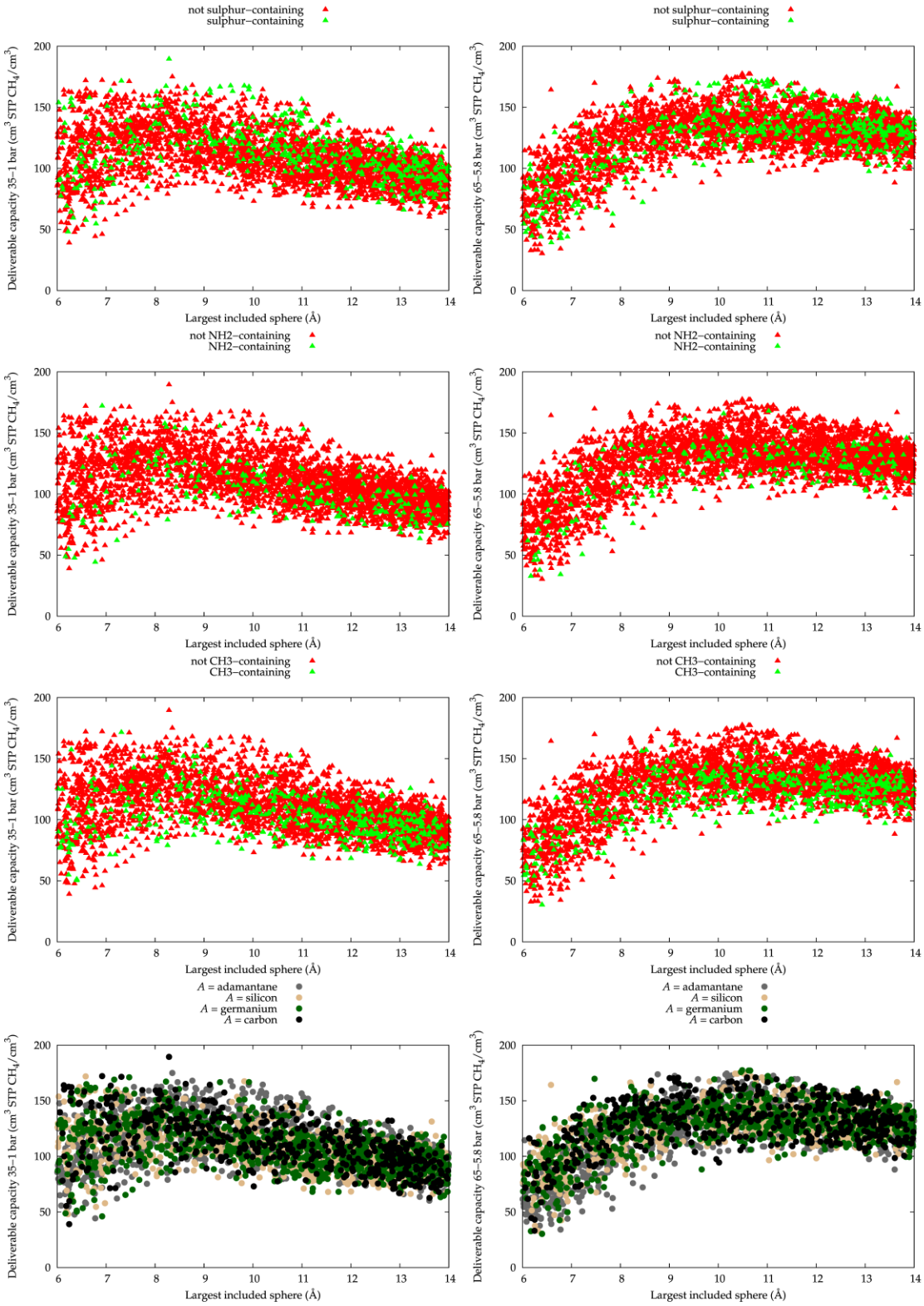

Figure S10. The deliverable capacity of materials (left: DC(35,1); right: DC(65,5.8)) within the broadly optimum pore diameter, categorized by chemical composition. From top to bottom: materials exhibiting sulfur atoms (the element with the strongest methane interaction within the force field utilized); NH_2 groups; CH_3 groups; and distinct *A* components.